Antarctic elevation drives hemispheric asymmetry in polar lapse-rate climatology and feedback

Authors: L. C. Hahn[1], K. C. Armour[1,2], D. S. Battisti[1], A. Donohoe[3], A. G. Pauling[1], and C. M. Bitz[1]

[1]Department of Atmospheric Sciences, University of Washington, Seattle, WA, USA.

[2]School of Oceanography, University of Washington, Seattle, WA, USA.

[3]Polar Science Center, Applied Physics Lab, University of Washington, Seattle, WA, USA.

Corresponding author: Lily Hahn (lchahn@uw.edu)

Key Points:

- Antarctic elevation causes asymmetry in climatological inversions, lapse-rate feedbacks, and warming between the poles
- In model experiments with flattened Antarctica, strengthened inversions lead to stronger lapse-rate feedback and Antarctic amplification
- Shortwave cloud feedback promotes seasonality in flat Antarctic warming; lapse-rate feedback more strongly promotes seasonality in Arctic

Abstract

The lapse-rate feedback is the dominant driver of stronger warming in the Arctic than the Antarctic in simulations with increased CO_2. While Antarctic surface elevation has been implicated in promoting a weaker Antarctic lapse-rate feedback, the mechanisms in which elevation impacts the lapse-rate feedback are still unclear. Here we suggest that weaker Antarctic warming under CO_2 forcing stems from shallower, less intense climatological inversions due to limited atmospheric heat transport above the ice sheet elevation and elevation-induced katabatic winds. In slab ocean model experiments with flattened Antarctic topography, stronger climatological inversions support a stronger lapse-rate feedback and annual-mean Antarctic warming comparable to the Arctic under CO_2 doubling. Unlike the Arctic, seasonality in warming over flat Antarctica is mainly driven by a negative shortwave cloud feedback which exclusively dampens summer warming, with a smaller contribution from the winter-enhanced lapse-rate feedback.

Plain Language Summary

Models project stronger surface warming in the Arctic than the Antarctic under climate change. A climate feedback in which more warming occurs near the surface than at higher altitudes in the atmosphere promotes this increased warming in the Arctic. Antarctica's surface elevation is thought to weaken this feedback in comparison to the Arctic, but how this occurs is unclear. Here we show that Antarctic elevation weakens surface warming by changing the base-state vertical temperature structure. When Antarctic topography is flattened in model experiments, Antarctica experiences more warming under climate change, resembling Arctic warming. Similarly to the Arctic, flat Antarctica warms most during the winter, but this seasonality is driven by different climate feedbacks in the Arctic versus Antarctic. These results indicate the importance of base-state temperatures for warming under climate change, and suggest that strong polar amplification is possible without local sea-ice loss.

1 Introduction

The Arctic has warmed about twice the global average in recent decades in a pattern known as Arctic amplification (Serreze et al., 2009; Screen and Simmonds, 2010a). In contrast, Antarctic amplification is not observed in the same timeframe, and Antarctic warming is dwarfed by Arctic warming in 21st century projections (Marshall et al., 2015; Smith et al., 2019). While Antarctic warming is delayed in part by Southern Ocean upwelling and associated heat uptake (Collins et al., 2013; Armour et al., 2016), global climate models also project weaker equilibrium warming for the Antarctic than the Arctic (e.g., Danabasoglu and Gent, 2009). In an evaluation of models in the fifth phase of the Coupled Model Intercomparison Project (CMIP5),

Goosse et al. (2018) find that the lapse-rate feedback is the single greatest factor contributing to this hemispheric asymmetry in polar warming.

In a warming climate, a positive polar lapse-rate feedback results from stable temperature inversions which contribute to stronger warming near the surface than aloft, leading to inefficient longwave emission to space. In the Arctic, the ice-albedo feedback promotes surface warming and thus contributes to a more-positive lapse-rate feedback (Feldl et al., 2017; Graversen et al., 2014). Dai et al. (2019) have more recently argued that Arctic sea-ice loss enables the lapse-rate feedback via increased turbulent heat fluxes and upward longwave radiation, enhancing lower-tropospheric warming over newly opened ocean. These results align with evidence that sea-ice loss promotes seasonality in Arctic warming by enhancing winter heat transfer from the ocean to the atmosphere and strengthening winter longwave radiative feedbacks (e.g., Screen and Simmonds, 2010b; Bintanja and van der Linden, 2013). Given the proposed dependence of Arctic lower-tropospheric warming and lapse-rate feedback on sea-ice loss, a weaker Antarctic lapse-rate feedback may be driven by the persistence of the Antarctic ice sheet.

Using fully-coupled Community Earth System Model (CESM) experiments, Salzmann (2017) instead finds that Antarctic elevation drives the weaker Antarctic lapse-rate feedback. As the sign and magnitude of the lapse-rate feedback depends on base-state static stability (Cronin and Jansen, 2015; Payne et al., 2015), we expect Antarctic elevation to control the lapse-rate feedback through impacts on base-state inversions. Confinement of the radiatively-active atmospheric column over Antarctica to a shallower layer than in the Arctic may additionally weaken the lapse-rate feedback.

With the mechanisms linking Antarctic elevation to a weaker lapse-rate feedback still unclear, we investigate hemispheric asymmetry in the polar lapse-rate feedback using slab ocean CESM experiments with present-day and flattened Antarctic topography under preindustrial and doubled CO_2. We analyze Antarctic elevation impacts on climatological inversions, the lapse-rate feedback, and polar amplification, in addition to investigating the seasonality of warming in the flat Antarctic compared to the Arctic. These experiments provide insight into hemispheric polar warming differences, with an ultimate goal of better understanding the mechanisms behind polar amplification.

2 Data and Methods

2.1 Model Experiments

To investigate hemispheric asymmetry in the lapse-rate feedback, we use CESM (Hurrell et al., 2013) version 1.2.2 with the Community Atmosphere Model version 4 (CAM4; Neale et al., 2013). CAM4 has a horizontal resolution of 0.9° x 1.25° and 26 vertical levels, with vertical grid spacing further described in Richter et al. (2014). For all experiments, CAM4 is coupled to a slab ocean forced with a spatially heterogeneous monthly climatology of ocean heat flux convergence derived from a fully-coupled preindustrial control simulation (Bitz et al., 2012). Differing from Salzmann (2017) in the use of a slab ocean rather than fully-coupled model, these experiments isolate the role of Antarctic elevation in determining the equilibrium climate response to CO_2 forcing and exclude potential effects of ocean heat uptake changes on the lapse-rate feedback (e.g., Po-Chedley et al., 2018; Singh et al., 2018). CESM also uses the Community Land Model version 4 (CLM4; Oleson et al., 2010) and the Los Alamos Sea Ice Model version 4 (CICE4; Hunke and Lipscomb, 2008).

We perform CESM experiments with present-day topography, referred to as the control Antarctic, or with the elevation of Antarctica flattened to 0 m above sea level, referred to as the flat Antarctic. Branching from preindustrial runs for the control and flat Antarctic, CO_2 is abruptly doubled from 285 to 570 ppm. We run each simulation for 50 years, and calculate climatologies over the final 30 years. Net top-of-atmosphere (TOA) energy imbalances of -0.09 W/m^2 (control, preindustrial), -0.06 W/m^2 (control, doubled CO_2), -0.14 W/m^2 (flat, preindustrial), and -0.09 W/m^2 (flat, doubled CO_2) indicate near equilibrium for all experiments in this period.

2.2 Radiative Feedbacks

We calculate the lapse-rate, Planck, surface-albedo, water-vapor, and cloud radiative feedbacks using the radiative kernel method (Shell et al., 2008; Soden et al., 2008). This method calculates radiative feedbacks as the product of (a) the change in radiative flux per unit change in a given climate variable, termed the radiative kernel, and (b) the modeled change in this climate variable normalized by the surface temperature change. While the Planck feedback is defined by propagating the surface temperature change through the entire troposphere, the lapse-rate feedback calculates the effect of departures from this vertically uniform temperature change. To calculate cloud feedbacks, the kernel method is used to determine the effect of noncloud variables (temperature, water vapor, and surface albedo) on the change in cloud radiative forcing (ΔCRF), and this cloud masking effect is subtracted from the total ΔCRF (Shell et al., 2008; Soden et al., 2008). We calculate the residual term by subtracting the kernel-estimated TOA radiation change from the modeled TOA radiation change, normalizing by the surface temperature change.

Following Goosse et al. (2018), we also calculate feedback contributions to polar warming (ΔTS) by dividing the energetic contribution of each feedback ($\lambda_i \Delta$TS), CO_2 forcing (F), change in atmospheric heat transport convergence (ΔAHT), and residual term (RΔTS) by the magnitude of the Planck response in either the control Antarctic (Figure 3b) or control Arctic (Figure 3c) ($\lambda_{p,c}$), where $\lambda'_p = \lambda_p - \lambda_{p,c}$ is the difference between the local Planck response (λ_p) and $\lambda_{p,c}$:

$$\Delta TS = -F/\lambda_{p,c} - \lambda'_p \Delta TS/\lambda_{p,c} - \sum_i \lambda_i \Delta TS/\lambda_{p,c} - \Delta AHT/\lambda_{p,c} - R\Delta TS/\lambda_{p,c} . \quad (1)$$

For this study, changes in climate variables are obtained from the doubled CO_2 minus preindustrial simulations, and radiative kernels are taken from Shell et al. (2008), calculated with an offline radiative transfer version of the Community Atmospheric Model, version 3 (CAM3). Feedbacks are calculated with respect to local rather than global surface temperature change (Armour et al., 2013; Feldl & Roe, 2013), and Arctic and Antarctic regional averages are defined for 70 to 90 ˚N and ˚S, respectively.

For the flat Antarctica experiment, we apply zonally averaged kernels from the Arctic between 60 and 90˚N to the flat Antarctic between 60 and 90˚S, shifted by six months. As the standard kernels do not exist below the Antarctic surface elevation, this allows for feedback calculation with the assumption that climate variable effects on TOA radiation for the flat Antarctic are similar to the Arctic. We note that radiative kernels are affected by climatological characteristics such as cloud patterns and land-ocean distributions, which differ between hemispheres. However, the flipped kernel method is supported by similar climatological winter temperature profiles in the flat Antarctic and control Arctic, with similar inversion depth and intensity (Section 3.1) and representative profiles (Figure S1a). We note that summer temperatures are colder in the flat Antarctic than the Arctic (Figure S1b) likely due to the

absence of leads over Antarctica. Nevertheless, both summer and winter demonstrate strong agreement between the modeled and kernel-estimated longwave (LW) TOA radiation change in the flat Antarctic (Figure S2). Annual LW and shortwave (SW) kernel-estimated changes in TOA radiation approximate the modeled TOA radiation change for the flat Antarctic almost as well as the control Antarctic experiments (Figure S3), further supporting this flipped kernel method. An alternative estimation of the SW feedbacks using the approximate partial radiative perturbation (APRP) technique (Taylor et al., 2007) produces control and flat Antarctic feedbacks that are qualitatively similar to those calculated using the kernel method (Figure S9).

2.3 Atmospheric Heat Transport

We calculate AHT across each latitude using the poleward integral of the difference between TOA and surface energy fluxes (and seasonal atmospheric energy storage for seasonal averages) from monthly model output (e.g., Kay et al., 2012; Donohoe et al., 2020a). We calculate latent heat transport as the poleward integral of evaporation minus precipitation at a given latitude, multiplied by the latent heat of vaporization, and dry static AHT as the residual between total AHT and latent AHT. As in Kay et al. (2012), we estimate polar AHT convergence by dividing the change in AHT at the edge of polar regions by the surface area of these regions. The change in AHT is then normalized by the Planck feedback for the AHT warming contribution and by the polar surface temperature change for the AHT feedback.

We also determine the vertical structure of AHT due to stationary eddies (SE) and transient eddies (TE) from CESM monthly output at 60˚N and 60˚S. For the vertical structure of TE transport, we neglect the potential energy term in Donohoe et al. (2020), which is small at high latitudes. Vertical structures of SE and TE are calculated as:

$$\mathrm{SE} = [\bar{V}^* \overline{MSE}^*] \quad (2)$$

and

$$\mathrm{TE} = \left[c_p\left(\overline{VT} - \overline{V}\,\overline{T}\right) + L\left(\overline{VQ} - \overline{V}\,\overline{Q}\right)\right], \quad (3)$$

where V is meridional velocity, MSE is moist static energy, c_p is the specific heat of air, L is the latent heat of vaporization of water, T is atmospheric temperature, and Q is specific humidity. Square brackets indicate zonal averages, overbars indicate monthly means, and asterisks denote departures from the zonal mean.

For comparison with CESM, we include vertical profiles of AHT and temperature from the ERA-Interim (Dee et al., 2011) and NCEP-NCAR (Kalnay et al. 1996) reanalyses, using 6-hourly fields for 1979-2018 to calculate SE and TE following Donohoe et al. (2020).

2.4 Inversion Depth and Intensity

Following Zhang et al. (2011), we define surface-based inversion depth as the geopotential thickness between the surface pressure and the first pressure level above which temperature decreases with height, and inversion intensity as the difference in temperature between these two levels.

3 Results

3.1 Climatological polar inversion asymmetry

Antarctic surface elevation drives modeled differences in base-state surface inversion depth and intensity between the poles. Using the CESM preindustrial control simulation during Arctic winter, Figure 1a shows a schematic of radiative-advective equilibrium, which controls base-state inversions in polar regions (Cronin and Jansen, 2015; Payne et al., 2015). In this framework, LW cooling and weak surface solar absorption promote cold near-surface temperatures, while poleward AHT (shown at 60˚N) maintains warmer temperatures aloft. As is also seen in the NCEP and ERA-Interim reanalyses (Figure S4), AHT supporting these

inversions maximizes in the lower troposphere (around 900 hPa), near the tropospheric temperature maximum. We propose that surface elevations above this level of maximum AHT promote shallower, radiatively-driven winter inversions in the Antarctic (Figure 1b).

This preindustrial temperature profile at 90°S demonstrates CESM's ability to resolve shallow surface inversions (here 50 hPa deep) matching radiosonde observations over the Antarctic Plateau, although the model underestimates the intensity of observed mean wintertime inversions which exceed 20 K at South Pole Station (Hudson & Brandt, 2005). Weaker winter inversions over coastal slopes in CESM (Figure 2a; Figure S5d) align well with coastal Antarctic radiosonde observations, which indicate typical depths shallower than 300 m and intensities less than 5 K (Zhang et al., 2011).

Considering CESM preindustrial winter inversion depth over the entire control Antarctic ice sheet, the deepest inversions are found where surface elevations are below the level of maximum poleward AHT (black contour, Figure 2a). Shallower winter inversions exist over the Antarctic Plateau, and inversion depth generally increases with increasing surface pressure over Antarctica (Figure 2b). Points with shallow inversions for a given surface pressure are located on (grey points, Figure 2b) or at the bottom of (boxed points, Figure 2b; stippling, Figure 2a) steep slopes (Figure S5a), where inversions may be disturbed by mixing due to katabatic winds (Vihma et al., 2011).

In contrast to Antarctica, most points in the Arctic are at higher surface pressures, allowing AHT to support deep inversions (Figure 2c, S5c). Inversions are shallower over the Greenland ice sheet, particularly over steep slopes, and in regions with low sea-ice fraction. While intense, shallow inversions (Figure S5d) exist at high Antarctic elevations, many areas show weaker inversion intensity than the Arctic (Figure S5f), especially over steep Antarctic

208 slopes. These inversions in CESM are consistent with radiosonde observations of generally
209 shallower, weaker inversions in the Antarctic compared to the Arctic (Zhang et al., 2011).
210 In comparison to the control Antarctic, inversions in the flat Antarctic preindustrial
211 experiment are intensified and deepened, particularly over steep slopes (Figures S5b,e, S6a,b).
212 An average inversion depth of 583 m and intensity of 7.5 K over the control Antarctic increases
213 to 846 m and 11.9 K over the flat Antarctic, more comparable with the average inversion depth
214 of 854 m and intensity of 9.0 K in the Arctic. We next investigate the extent to which these
215 stronger, deeper climatological inversions in the flat Antarctic simulation, which more closely
216 resemble Arctic inversions, may promote an Arctic-like lapse-rate feedback and stronger
217 Antarctic amplification.
218 3.2 Polar amplification and lapse-rate feedback asymmetry
219 In contrast to control Antarctic warming (5.4 K) under doubled CO_2, flat Antarctic
220 warming (6.3 K) is more comparable to control Arctic warming (6.7 K; Figure 3a) in the annual
221 mean. Applying Eq. (1), we find that the largest contributor to stronger amplification in the flat
222 Antarctic is the lapse-rate feedback (Figure 3b). A more-positive water-vapor feedback and
223 ΔAHT also support enhanced flat Antarctic warming, while more-negative Planck and cloud
224 feedbacks and a less-positive albedo feedback oppose flat Antarctic warming. The LW residual
225 term is similar for the control and flat Antarctic, although the SW residual term is slightly larger
226 in the flat Antarctic (Figure S7a). Flat Antarctica experiences lapse-rate, water-vapor, and Planck
227 warming contributions nearly equivalent to the Arctic, while a larger ΔAHT and residual term
228 in the flat Antarctic partly balance more-positive albedo and cloud feedbacks in the Arctic
229 (Figure 3c).

Figures S7b-g show the response to CO_2 doubling for flat minus control Antarctic topography experiments for various climate variables relevant for feedbacks (left) and the difference for the radiative kernels (right), where *T* is atmospheric temperature, *TS* is surface temperature, *q* is specific humidity, and α is albedo. The strengthened lapse-rate feedback in the flat Antarctic is supported both by more surface-trapped warming in response to CO_2 doubling (more-negative $\Delta(T\text{-}TS)$), and by a more-negative *T* kernel due to deepening and moistening the atmospheric column (Figure S7b,c). While it is difficult to quantify exactly how much of the increased lapse-rate feedback in the flat versus control Antarctic stems from the deeper troposphere alone, we find that only 26% of this increase can be obtained from simply extending the control Antarctic $\Delta(T\text{-}TS)$ from the lowest elevations above the ice sheet to all pressure levels below the ice sheet and multiplying by the flat Antarctic temperature kernel. This suggests that the increased lapse-rate feedback over flat Antarctica is strongly driven by enhanced surface-trapped warming, rather than simply a deeper atmospheric column.

Surface-trapped warming enhancement for the flat Antarctic appears largest over the Transantarctic Mountains and coastal slopes, where steep slopes promote shallow, weak inversions in the control topography experiment (Figure S7b). Particularly for these regions, increased preindustrial inversion depth and intensity in the flat experiment support stronger low-level warming (Figure S6) and an enhanced lapse-rate feedback.

Both the stronger water-vapor feedback and weaker surface-albedo feedback in the flat Antarctic are supported by deepening and moistening the atmospheric column. This amplifies the greenhouse effect of water vapor by increasing the column-integrated specific humidity and strengthening the water-vapor kernel (Figure S7d,e). The deeper atmospheric column over flat Antarctica also dampens surface albedo impacts on TOA radiation, and this weaker (less-

253 negative) albedo kernel (Figure S7g) drives a weakened albedo feedback in the flat Antarctic.
254 Since feedbacks are normalized by local surface temperature change, the more-negative flat
255 Antarctic Planck feedback shown in Figure S7a can be attributed to a stronger atmospheric
256 temperature kernel due to a warmer, deeper emitting column.

257 The more-negative cloud feedback in the flat versus control Antarctic is explained by
258 more-negative SW cloud forcing (Figure S8a; Figure S11aa). The flat Antarctic experiences a
259 larger increase in cloud cover and cloud water path due to increased low-level liquid-bearing
260 clouds under CO_2 doubling (Figure S8d,e), supporting a stronger negative SW cloud feedback.
261 Preindustrial cloud water path (not shown) is also larger for the flat Antarctic, likely due to an
262 extended lower atmosphere, enhanced water-vapor transport, and increased stability. Areas of
263 stronger sea-ice loss (Figure S8c) for the flat Antarctic also correspond to increased cloud
264 water path and SW forcing.

265 Increased preindustrial AHT toward the Antarctic balances stronger cooling to space
266 over flat Antarctica (Figure S10a), consistent with Singh et al. (2016) and Salzmann (2017).
267 Under doubled CO_2, AHT to the flat Antarctic also increases more, largely due to enhanced
268 southward latent AHT (Figure S10b). ΔAHT and feedback calculations for these slab ocean
269 experiments using the kernel method produce similar results to Salzmann (2017), who employ
270 partial radiative perturbation (PRP) feedback computations for the transient response to CO_2
271 doubling in fully-coupled runs: flat Antarctica experiences stronger lapse-rate and water-vapor
272 feedbacks and increased poleward ΔAHT, opposed by more-negative Planck and cloud
273 feedbacks and a less-positive albedo feedback.

274 3.3 Radiative feedback contributions to seasonality in Arctic and Antarctic amplification

Enhanced warming in the flat Antarctic compared with the control topography experiment occurs predominantly during the winter season (Figure 4a-c), with similar summer warming for flat and control experiments. This produces a greater difference between winter and summer warming (4.0 K) in the flat Antarctic compared to the elevated Antarctic (2.1 K), more comparable with control Arctic warming seasonality (5.3 K). To investigate what causes enhanced seasonality in warming in the flat Antarctic experiment, we compare winter and summer climate feedbacks. Feedbacks shown are normalized by the annual-mean local warming, although we find similar results for normalizing by seasonal warming. Figures 4d-i highlight seasonal lapse-rate and SW cloud feedbacks, with seasonality for all feedbacks shown in Figure S11.

In the Arctic, the lapse-rate feedback strongly promotes greater warming in winter than summer (Figure 4f), consistent with Pithan and Mauritsen (2014). This enhanced winter lapse-rate feedback is driven by stronger base-state inversions in winter compared to summer, when sea-ice melting keeps surface temperatures near the freezing point. While strong lapse-rate feedback seasonality occurs over Southern Ocean sea ice, seasonality in this feedback is weaker over Antarctica for both the control and flat experiments. Flat Antarctica experiences stronger seasonality in warming than control Antarctica due in part to strengthened winter inversions, but the primary feedback enhancing flat Antarctic warming seasonality is the SW cloud feedback.

Due to polar night during winter, enhanced SW cloud cooling in the flat Antarctic occurs exclusively during summer (Figure 4h). While the lapse-rate and water-vapor feedbacks promote greater warming for the flat Antarctic throughout the year, greater warming seasonality over flat Antarctica results largely from the SW cloud feedback damping only

298 summertime warming. About two thirds of the difference in SW cloud feedback seasonality
299 between control and flat Antarctica arises from cloud radiative forcing, with the other third
300 coming from differences in the cloud masking term. A weaker summer surface albedo feedback
301 over flat Antarctica also contributes slightly to stronger winter versus summer warming, with
302 stronger albedo feedback seasonality changes over sea ice (Figure S11d).

303 **4 Conclusions**

304 With a goal of understanding the mechanisms driving lapse-rate feedback differences
305 between the Arctic and Antarctic, we compare CESM slab ocean experiments with control and
306 flattened Antarctic topography under preindustrial and doubled CO_2 forcing. We find
307 climatological differences in CESM preindustrial Arctic and Antarctic inversions, supported by
308 radiosonde observations. Limited poleward atmospheric heat transport above ice sheet
309 elevations, in addition to mixing due to katabatic winds on steep slopes, drives shallower,
310 weaker inversions for the Antarctic than the Arctic. Combined with weaker emission from the
311 relatively shallow and dry Antarctic atmospheric column, these weaker Antarctic inversions
312 prohibit the strong positive lapse-rate feedback seen in the Arctic. In contrast, over the flat
313 Antarctic, stronger climatological inversions support a lapse-rate feedback that is comparable to
314 that in the Arctic, with nearly equivalent degrees of polar amplification in each hemisphere in
315 these slab ocean experiments. While the seasonality of warming in the flat Antarctic is also
316 more comparable to the Arctic, this seasonality is supported by different climate feedbacks at
317 each pole: lapse-rate feedback seasonality contributes strongly to enhanced winter warming in
318 the Arctic, while a negative SW cloud feedback that only applies to non-winter months
319 contributes more to flat Antarctic seasonality.

As noted by Salzmann (2017), enhanced Antarctic amplification in flat Antarctica experiments suggests that reduced Antarctic surface elevation due to mass loss would accelerate Antarctic amplification under climate change. In the context of previous studies considering the relative roles of sea ice and the lapse-rate feedback for polar amplification (e.g., Graversen et al., 2014; Dai et al., 2019), investigating Antarctic amplification can also provide insight into mechanisms supporting Arctic amplification. Flat Antarctic experiments here and in Salzmann (2017) demonstrate that strong, Arctic-like polar amplification is possible without local sea-ice loss, although non-local sea-ice loss in the Southern Ocean likely contributes to Antarctic amplification through changes in AHT. Our experiments additionally indicate that the strongest seasonality in the lapse-rate feedback occurs in regions with sea ice: even over the flattened Antarctic continent, lapse-rate feedback seasonality pales in comparison to lapse-rate feedback seasonality over the Southern Ocean and Arctic. In line with Cronin and Jansen (2015) and Payne et al. (2015), enhanced flat Antarctic warming supports the dependence of the lapse-rate feedback on base-state inversions, which themselves depend on sea-ice concentration and surface albedo in the Arctic. Further work to disentangle the lapse-rate feedback from sea-ice effects may clarify how they will change separately and in tandem under climate change.

Acknowledgments

LCH was supported by the National Science Foundation (NSF) Graduate Research Fellowship Grant DGE-1762114. KCA was supported by NSF Awards AGS-1752796 and OCE-1850900. AD was supported by the NSF Antarctic Program Grant PLR 1643436. CMB and ASP were supported by the National Science Foundation Antarctic Program Grant OPP-1602435. We acknowledge high-performance computing support from Cheyenne and data storage provided by NCAR's Computational and Information Systems Laboratory (2019), sponsored by the NSF. CESM model output relevant for study figures is available at https://doi.org/10.5281/zenodo.3735441 (Hahn et al., 2020). ERA-Interim data was provided by the ECMWF Data Archive at https://apps.ecmwf.int/datasets/data/interim-full-daily/levtype=pl/, and NCEP data was provided at https://www.esrl.noaa.gov/psd/ by the NOAA/OAR/ESRL PSD, Boulder, Colorado.

References

Armour, K. C., Bitz, C. M., & Roe, G. H. (2013). Time-varying climate sensitivity from regional feedbacks. *Journal of Climate*, *26*, 4518–4534. https://doi.org/10.1175/JCLI-D-12-00544.1

Armour, K. C., Marshall, J., Scott, J., Donohoe A., & Newsom, E. R. (2016). Southern Ocean warming delayed by circumpolar upwelling and equatorward transport. *Nature Geoscience*, *9*, 549–554. https://doi.org/10.1038/ngeo2731

Bintanja, R., & van der Linden, E. (2013). The changing seasonal climate in the Arctic. *Scientific Reports, 3*, 1556. https://doi.org/10.1038/srep01556

Bitz, C.M., Shell, K.M., Gent, P.R., Bailey, D.A., Danabasoglu, G., Armour, K.C., Holland, M.M., & Kiehl, J.T. (2012). Climate Sensitivity of the Community Climate System Model, Version 4. *Journal of Climate, 25*, 3053–3070. https://doi.org/10.1175/JCLI-D-11-00290.1

Collins, M., Knutti, R., Arblaster, J., Dufresne, J-L., Fichefet, T., Friedlingstein, P., et al. (2013). Long-term climate change: Projections, commitments and irreversibility. In T. F. Stocker, D. Qin, G-K. Plattner, M. M. B. Tignor, S. K. Allen, J. Boschung, et al. (Eds.), *Climate Change 2013 - The Physical Science Basis: Contribution of Working Group I to the Fifth Assessment Report of the Intergovernmental Panel on Climate Change* (pp. 1029-1136). (Intergovernmental Panel on Climate Change). New York, NY: Cambridge University Press.

Computational and Information Systems Laboratory (2019). Cheyenne: HPE/SGI ICE XA System (Climate Simulation Laboratory). Boulder, CO: National Center for Atmospheric Research. https://doi.org/10.5065/D6RX99HX

Cronin, T. W., & Jansen, M. F. (2016). Analytic radiative-advective equilibrium as a model for high-latitude climate. *Geophysical Research Letters*, *43*, 449–457. https://doi.org/10.1002/2015GL067172

Danabasoglu, G., & Gent, P.R. (2009). Equilibrium climate sensitivity: Is it accurate to use a slab ocean model? *Journal of Climate*, *22*, 2494–2499. https://doi.org/10.1175/2008JCLI2596.1

Dai, A., Luo, D., Song, M., & Liu, J. (2019). Arctic amplification is caused by sea-ice loss under increasing CO_2. *Nature Communications, 10*, 121. https://doi.org/10.1038/s41467-018-07954-9

Dee, D. P., Uppala, S. M., Simmons, A. J., Berrisford, P., Poli, P., Kobayashi, S., et al. (2011). The ERAInterim reanalysis: Configuration and performance of the data assimilation system. *Quarterly Journal of the Royal Meteorological Society*, *137*, 553–597. https://doi.org/10.1002/qj.828

Donohoe, A., Armour, K. C., Roe, G. H., Battisti, D. S., & Hahn, L. (2020). The partitioning of meridional heat transport from the Last Glacial Maximum to CO_2 quadrupling in coupled climate models. *Journal of Climate, 33,* 4141-4165. https://doi.org/10.1175/JCLI-D-19-0797.1

Feldl, N., & Roe, G. H. (2013). Four perspectives on climate feedbacks. *Geophysical Research Letters, 40*, 4007–4011. https://doi.org/10.1002/grl.50711

Feldl, N., Bordoni, S., & Merlis, T. M. (2017). Coupled high-latitude climate feedbacks and their impact on atmospheric heat transport. *Journal of Climate*, *30*, 189–201. https://doi.org/10.1175/JCLI-D-16-0324.1

Goosse, H., Kay, J. E., Armour, K. C., Bodas-Salcedo, A., Chepfer, H., Docquier, D., et al. (2018). Quantifying climate feedbacks in polar regions. *Nature Communications*, *9*, 1919. https://doi.org/10.1038/s41467-018-04173-0

Graversen, R. G., Langen, P. L., & Mauritsen, T. (2014). Polar amplification in CCSM4: Contributions from the lapse rate and surface albedo feedbacks. *Journal of Climate*, *27*, 4433–4450. https://doi.org/10.1175/JCLI-D-13-00551.1

Hahn, L. C., Armour, K. C., Battisti, D. S., Donohoe, A., Pauling, A. G., & Bitz, C. M. (2020). Supporting Data for Hahn et al. GRL: Antarctic elevation drives hemispheric asymmetry in polar lapse-rate climatology and feedback [Data set]. Zenodo. http://doi.org/10.5281/zenodo.3735442

Hudson, S. R., & Brandt, R. E. (2005). A look at the surface-based temperature inversion on the Antarctic Plateau. *Journal of Climate*, *18*, 1673–1696. https://doi.org/10.1175/JCLI3360.1

Hunke, E., & Lipscomb, W. (2008). CICE: The Los Alamos sea ice model, documentation and software, version 4.0 (Tech. Rep. LA-CC-06-012). Los Alamos, NM: Los Alamos National Laboratory.

Hurrell, J. W., Holland, M. M., Gent, P. R., Ghan, S., Kay, J. E., Kushner, P. J., et al. (2013). The Community Earth System Model: A framework for collaborative research. *Bulletin of the American Meteorological Society*, *94*(9), 1339–1360. https://doi.org/10.1175/BAMS-D-12-00121.1

Kalnay, E., Kanamitsu, M., Kirtler, R., Collins, W., Deaven, D., Gandin, L., et al. (1996). The NCEP/NCAR 40-year reanalysis project. *Bulletin of the American Meteorological Society, 77*(3), 437– 471. https://doi.org/10.1175/1520-0477(1996)077<0437:TNYRP>2.0.CO;2

Kay, J. E., Holland, M. M., Bitz, C. M., Blanchard-Wrigglesworth, E., Gettelman, A., Conley, A., & Bailey, D. (2012). The influence of local feedbacks and northward heat transport on the equilibrium Arctic climate response to increased greenhouse gas forcing. *Journal of Climate*, *25*(16), 5433–5450. https://doi.org/10.1175/jcli-d-11-00622.1

Marshall, J., Scott, J.R., Armour, K.C., Campin, J.-M., Kelley, M., & Romanou, A. (2015). The ocean's role in the transient response of climate to abrupt greenhouse gas forcing. *Climate Dynamics, 44,* 2287–2299. https://doi.org/10.1007/s00382-014-2308-0

Neale, R. B., Richter, J., Park, S., Lauritzen, P. H., Vavrus, S. J., Rasch, P. J., & Zhang, M. (2013). The mean climate of the Community Atmosphere Model (CAM4) in forced SST and

fully coupled experiments. *Journal of Climate*, *26*, 5150–5168. https://doi.org/10.1175/JCLI-D-12-00236.1

Oleson, K., Lawrence, D., Bonan, G., Flanner, M., Kluzek, E., Lawrence, P., et al. (2010). Technical description of version 4.0 of the Community Land Model (CLM) (Tech. Rep. TN-478+STR). Boulder, CO: National Center for Atmospheric Research.

Payne, A. E., Jansen, M. F., & Cronin, T. W. (2015). Conceptual model analysis of the influence of temperature feedbacks on polar amplification. *Geophysical Research Letters*, *42*, 9561–9570. https://doi.org/10.1002/2015GL065889

Pithan, F., & Mauritsen, T. (2014). Arctic amplification dominated by temperature feedbacks in contemporary climate models. *Nature Geoscience, 7*, 181–184. https://doi.org/10.1038/ngeo2071

Po-Chedley, S., Armour, K. C., Bitz, C. M., Zelinka, M. D., Santer, B. D., & Fu, Q. (2018). Sources of intermodel spread in the lapse rate and water vapor feedbacks. *Journal of Climate*, *31*(8), 3187–3206. https://doi.org/10.1175/JCLI-D-17-0674.1

Richter, J. H., Solomon, A., & and Bacmeister, J. T. (2014). Effects of vertical resolution and nonorographic gravity wave drag on the simulated climate in the Community Atmosphere Model, version 5. *Journal of Advances in Modeling Earth Systems*, *6*, 357–383. https://doi.org/10.1002/2013MS000303

Salzmann, M. (2017). The polar amplification asymmetry: role of Antarctic surface height. *Earth System Dynamics*, *8*, 323–336. https://doi.org/10.5194/esd-8-323-2017

Screen, J. A., & Simmonds, I. (2010a). The central role of diminishing sea ice in recent Arctic temperature amplification. *Nature*, *464*, 1334–1337. https://doi.org/10.1038/nature09051

Screen, J. A., & Simmonds, I. (2010b). Increasing fall-winter energy loss from the Arctic Ocean and its role in Arctic temperature amplification. *Geophysical Research Letters, 37*, L16707. https://doi.org/10.1029/2010GL044136

Serreze, M. C., Barrett, A. P., Stroeve, J. C., Kindig, D. N., & Holland, M. M. (2009). The emergence of surface-based Arctic amplification. *The Cryosphere*, *3*, 11–19. https://doi.org/10.5194/tc-3-11-2009

Shell, K. M., Kiehl, J. T., & Shields, C. A. (2008). Using the radiative kernel technique to calculate climate feedbacks in NCAR's Community Atmospheric Model. *Journal of Climate*, *21*, 2269–2282. https://doi.org/10.1175/2007JCLI2044.1

Singh, H. A., Bitz, C. M., & Frierson, D. M. W. (2016). The global climate response to lowering surface orography of Antarctica and the importance of atmosphere-ocean coupling. *Journal of Climate, 29*(11), 4137–4153. https://doi.org/10.1175/JCLI-D-15-0442.1

Singh, H., Garuba, O., & Rasch, P. (2018). How asymmetries between Arctic and Antarctic climate sensitivity are modified by the ocean. *Geophysical Research Letters*, *45*, 13,031–13,040. https://doi.org/10.1029/2018GL079023

Smith, D. M., Screen, J. A., Deser, C., Cohen, J., Fyfe, J. C., García-Serrano, J., et al. (2019). The Polar Amplification Model Intercomparison Project (PAMIP) contribution to CMIP6: investigating the causes and consequences of polar amplification. *Geoscientific Model Development*, *12*, 1139–1164. https://doi.org/10.5194/gmd-12-1139-2019

Soden, B. J., Held, I. M., Colman, R., Shell, K. M., Kiehl, J. T., & Shield, C. A. (2008). Quantifying climate feedbacks using radiative kernels. *Journal of Climate*, *21*, 3504–3520. https://doi.org/10.1175/2007JCLI2110.1

Taylor, K. E., Crucifix, M., Braconnot, P., Hewitt, C. D., Doutriaux, C., Broccoli, A. J., Mitchell, J. F. B., & Webb, M. J. (2007). Estimating Shortwave Radiative Forcing and Response in Climate Models. *Journal of Climate*, *20*, 2530–2543. https://doi.org/10.1175/JCLI4143.1

Vihma, T., Tuovinen, E., & Savijärvi, H. (2011). Interaction of katabatic winds and near-surface temperatures in the Antarctic. *Journal of Geophysical Research*, *116*, D21119. https://doi.org/10.1029/2010JD014917

Zhang, Y., Seidel, D. J., Golaz, J. C., Deser, C., & Tomas, R. A. (2011). Climatological characteristics of Arctic and Antarctic surface-based inversions. *Journal of Climate, 24*(19), 5167–5186. https://doi.org/10.1175/2011JCLI4004.1

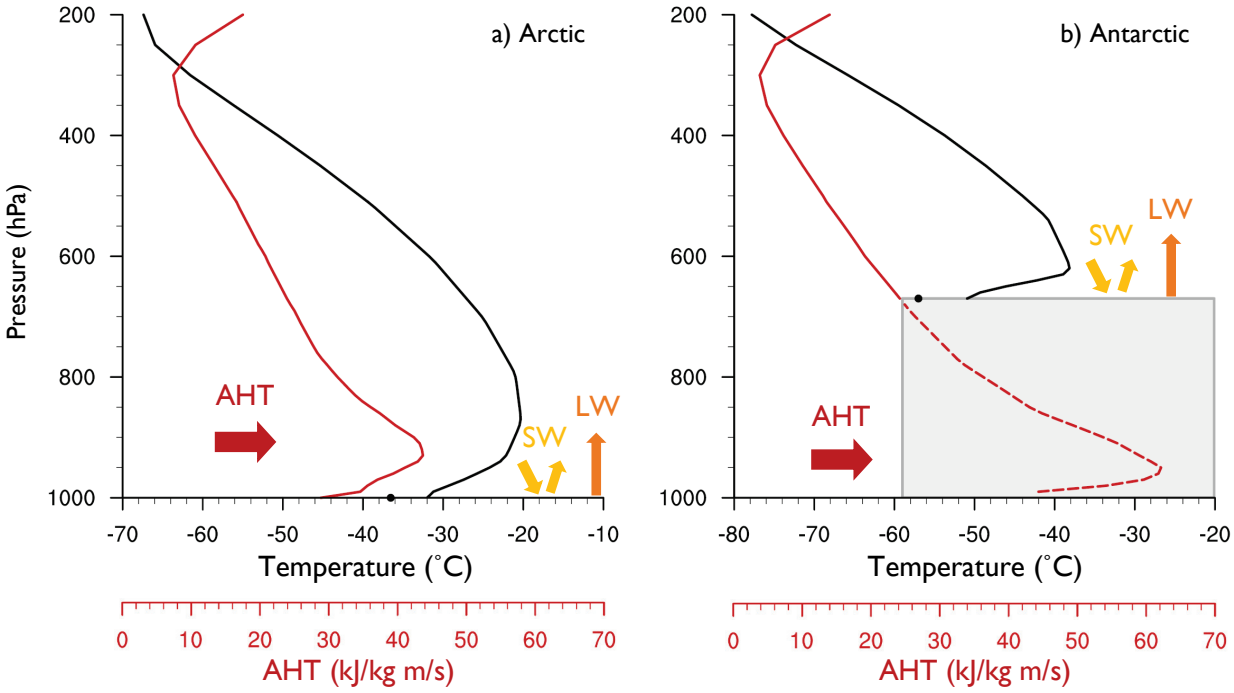

Figure 1. Radiative-advective equilibrium schematic using the CESM preindustrial control topography temperature and AHT. Vertical profiles of winter poleward AHT due to transient and stationary eddies at (a) 60˚N and (b) 60˚S (red; kJ/kg m/s) and winter temperature at (a) 90˚N and (b) 90˚S (black; dot for surface temperature; ˚C).

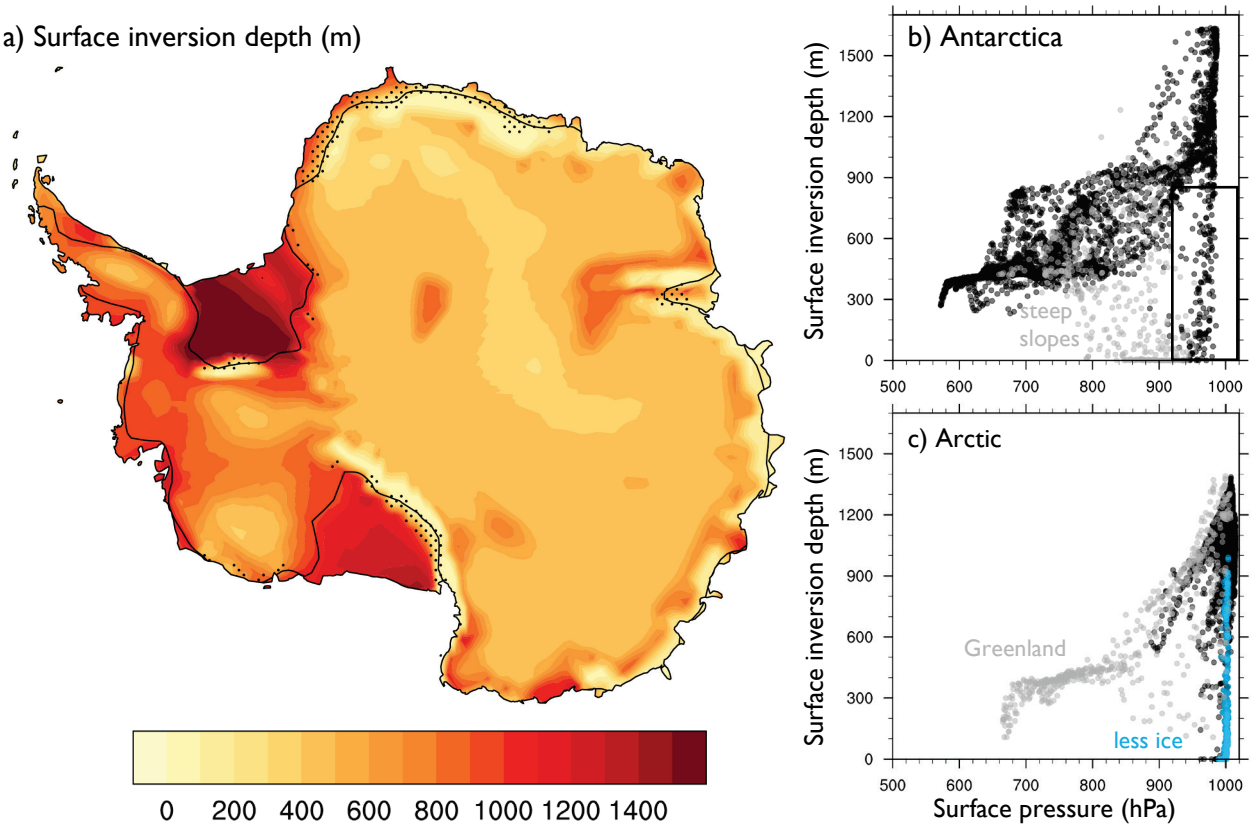

Figure 2. Winter surface-based inversion depth (m) for (a) Antarctica, (b) Antarctica from 70 to 90˚S, and (c) the Arctic from 70 to 90˚N from the CESM preindustrial control topography experiment. Black contour in (a) shows where the winter surface pressure equals 950 hPa: the level of the maximum AHT due to transient and stationary eddies during winter at 60˚S. Grey points in (b) indicate surface slopes greater than .007. Boxed points in (b), with surface pressure greater than 920 hPa and inversion depth less than 850 m, correspond to stippled regions in (a). In (c), blue points indicate winter sea ice fraction less than .97, and grey points are located over Greenland.

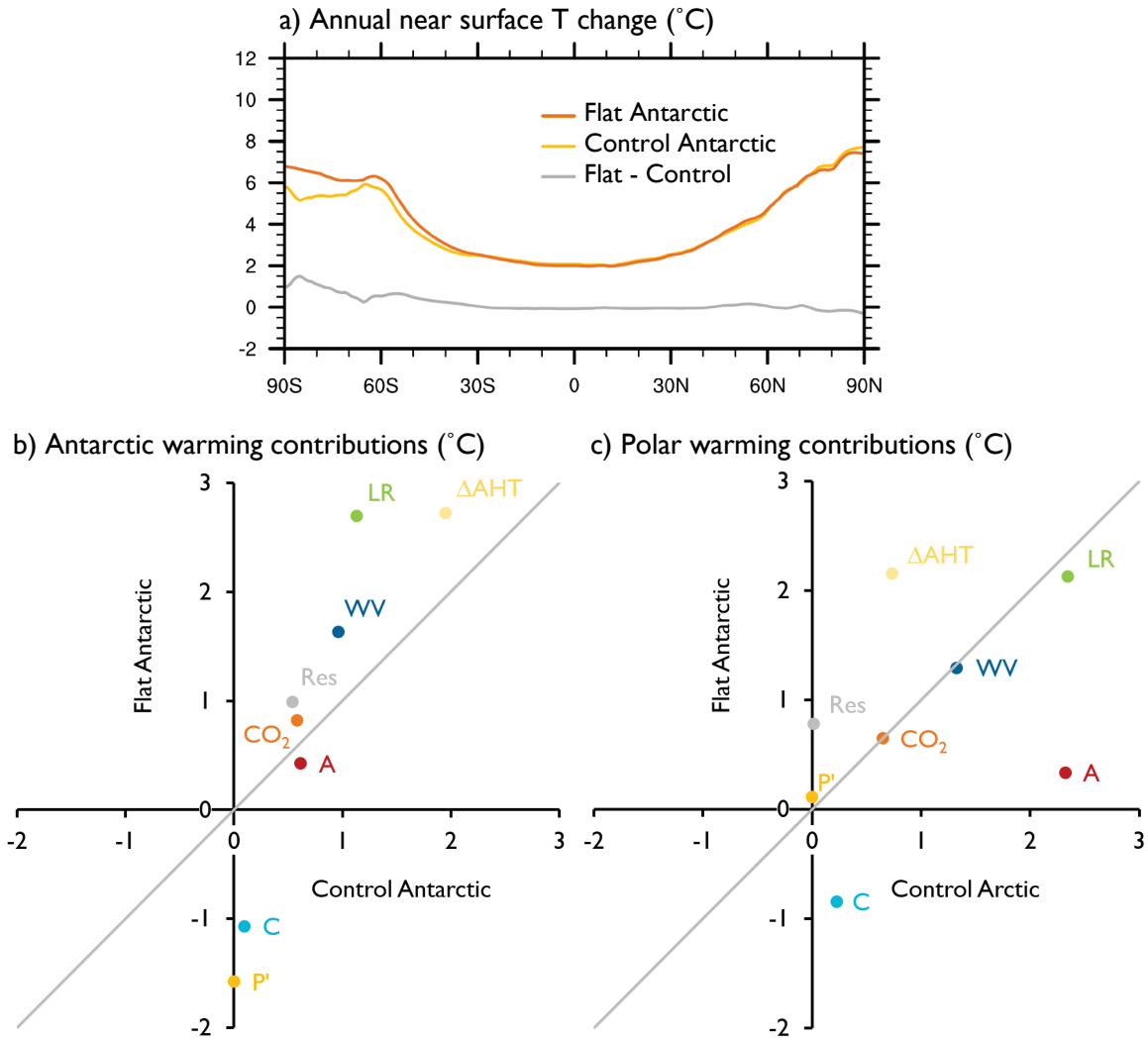

Figure 3. (a) Zonal- and annual-mean near-surface temperature change (˚C) under CO_2 doubling in the control (yellow) and flat (orange) Antarctic experiments and their difference (grey); (b,c) Contributions of each feedback and atmospheric forcing to warming (˚C) for the flat Antarctic compared to (b) the control Antarctic and (c) the control Arctic for the lapse rate (LR), surface albedo (A), water vapor (WV), and cloud (C) feedbacks, the variation in the Planck response from its value in (b) the control Antarctic and (c) the control Arctic (P'), CO_2 forcing (CO_2), change in AHT convergence (ΔAHT), and residual term (Res).

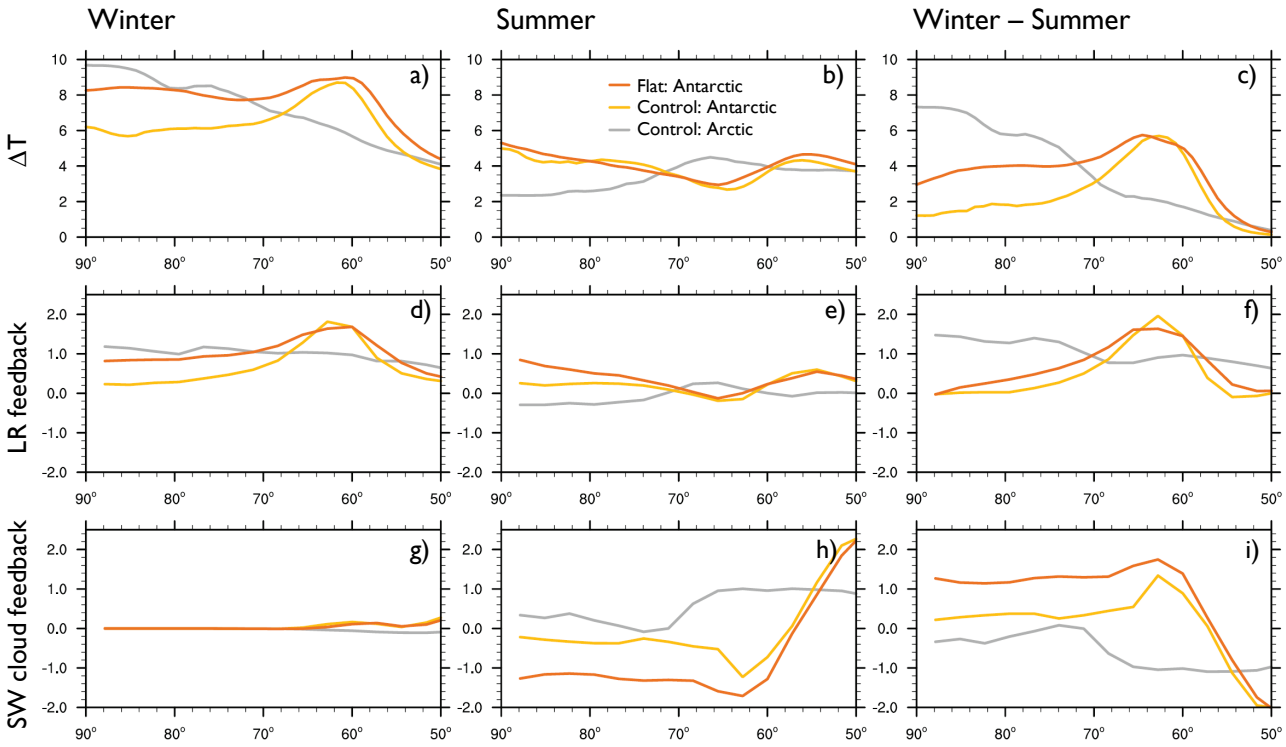

Figure 4. Zonal-mean (a-c) near surface temperature change (˚C), (d-f) lapse rate feedback ($W/m^2/K$), and (g-i) shortwave (SW) cloud feedback ($W/m^2/K$) under CO_2 doubling in the control Arctic (grey) and control (yellow) and flat (orange) Antarctic for (a,d,g) winter, (b,e,h) summer, and (c,f,i) winter minus summer.